Materials Transactions, Vol. 43, No. 8 (2002) pp. 1892 to 1906
Special Issue on Bulk Amorphous, Nano-Crystalline and Nano-Quasicrystalline Alloys IV

OVERVIEW

Recent Progress in Bulk Glassy Alloys

Akihisa Inoue and Akira Takeuchi

Institute for Materials Research, Tohoku University, Sendai 980-8577, Japan

This paper deals with recent progress in stabilized supercooled liquid and the resulting bulk glassy alloys and focusing on the following factors; alloy composition, forming ability, formation mechanism, computed glass-forming ability, computed glass formation range, atomic configuration, production techniques, mechanical properties, corrosion resistance, soft magnetic properties, micro-forming ability, applications, significance to science and engineering, and future trends for bulk glassy alloys including supercooled liquid. As demonstrated in this review, the high stability of metallic supercooled liquid has already opened up new fields of investigation in basic science and yielded new engineering applications. There is every reason to expect that their importance will continue to increase.

(Received February 13, 2002; Accepted April 17, 2002)

Keywords: *bulk metallic glasses, high glass-forming ability, formation process, component rule, formation mechanism, computed estimation, engineering property, micro-forming, application*

1. Introduction

For thousands of years, metallic alloys have been among the most important materials used by mankind, and their importance as engineering materials remains as great now as ever. Without exception, all bulk metallic alloys used to date consist of crystalline materials with three-dimensional periodic atomic configurations. The instability of the liquid phase of metallic alloys below melting temperature had been thought to be a universal phenomenon, making the formation of a crystalline phase of the bulk metallic alloy unavoidable. In order to prevent transition from a liquid to a crystalline phase, extremely high cooling rates of the order 10^6 K/s are required and the alloys exhibiting critical cooling rates of 10^5 to 10^7 K/s are known as amorphous/glass forming alloys.[1,2] As a result of the requirement for rapid cooling, amorphous alloys have usually been produced in a thin sheet form with thicknesses below 0.05 mm. The conventionally accepted concept that the supercooled liquid phase of metallic alloys is always unstable has been broken through by the recent successes in forming bulk glassy alloys in a number of transition metal-based alloy systems using the copper mold casting technique.[3–5] In recent years, studies of the stabilization of metallic supercooled liquid and the resulting bulk glassy alloys have been significant not only for fundamental science but for engineering applications as well. In this paper we review our recent results on the formation and properties of bulk glassy alloys.

2. Bulk Glassy Alloy Systems

Figure 1 summarizes the critical cooling rate (R_c), maximum sample thickness (t_{max}) and reduced glass transition temperature (T_g/T_m) relationship for bulk glassy alloys developed over the last decade, together with the previous data on ordinary amorphous alloys in Fe-, Co- and Ni-based systems and Pd- and Pt-based glassy alloys.[4] It is well known that Fe-, Co- and Ni-based amorphous alloys found before 1988 require high cooling rates above 10^5 K/s for the formation of an amorphous phase and the resulting sample thickness is limited to less than about 0.05 mm.[2] As an exceptional this, it is known that Pd–Ni–P and Pt–Ni–P alloys have low critical cooling rates in the order of 10^3 K/s and bulk glassy alloys are formed in a diameter range up to 2 mm by water quenching.[1] Recently, new multi-component glassy alloys with much lower critical cooling rates for glass formation were found in Ln-,[6] Mg-,[7] Zr-,[8,9] Ti-,[10] Fe-,[11] Pd-[12] and Cu-[13] based systems. At present, the lowest critical cooling rate is as low as 0.06 K/s[14] and the largest sample thickness is expected to be as large as about 150 mm, though the largest experimental diameter achieved so far is 80 mm.[15] Additionally, one can see that these new bulk glassy alloys have high T_g/T_m above 0.7 and the highest T_g/T_m value reaches 0.74.[12] By choosing these new alloy compositions, one can produce rather easily bulk glassy alloys by various simple processes

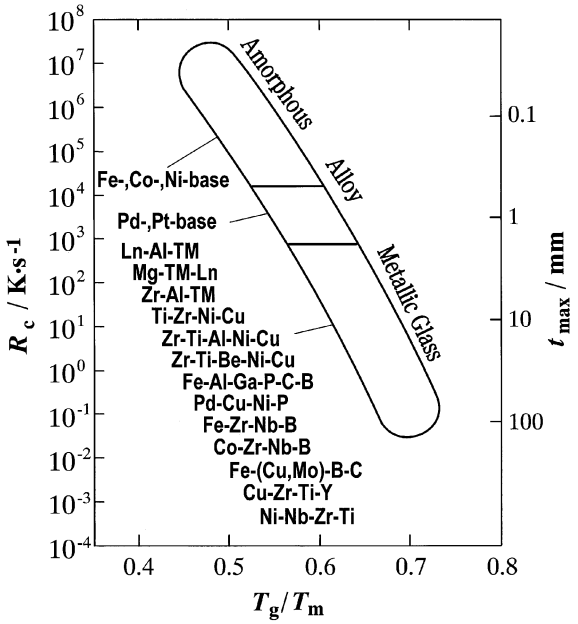

Fig. 1 Critical cooling rate (R_c), maximum sample thickness (t_{max}) and reduced glass transition temperature (T_g/T_m) relationship for bulk glassy alloys developed over the last decade, together with the previous data on ordinary amorphous alloys in Fe-, Co- and Ni-based systems and Pd- and Pt-based glassy alloys.[4]

such as water quenching, arc-melt casting and conventional copper mold casting.[3] It has previously been demonstrated that one can obtain a cylindrical rod of 16 mm in diameter and 600 mm in length with a Zr–Al–Ni–Cu system and a cylindrical ingot of 75 mm in diameter and 85 mm in length with a Pd–Cu–Ni–P system.[5]

Table 1 summarizes typical bulk glassy alloy systems reported to date together with the calendar years when the first paper and/or patent for each alloy system was published. The glassy alloy systems can be divided into nonferrous and ferrous types. Among the nonferrous alloy systems with a maximum diameter above 5 mm, one can list Mg–Ln–(Ni, Cu),[16] Ln–Al–(Ni, Cu),[17] Zr–Al–(Ni, Cu),[18] Zr–Al–(Ni, Cu) containing Ti, Nb, Ta or Pd,[19] Zr–Ti–Be–Ni–Cu,[9] Pd–Cu–Ni–P,[12] Pd–Cu–Fe–P,[20] Ti–Ni–Cu–Sn,[21] Cu–Zr–Ti–Y[22] and Cu–Zr–Ti–Be[23] systems. On the other hand, Fe- and Co-based alloy systems with a maximum diameter above 2 mm are mainly composed of Fe–(Al, Ga)–(P, C, B),[11] Fe–(Al, Ga)–(P, C, B) containing Cr, Mo or Nb,[24] Fe–Ga–(P, C, B),[25] Fe–Ga–(P, C, B)–(Cr, Mo),[26] Fe–(Zr, Hf, Nb)–B,[27] Fe–Co–Ln–B,[28] Fe–(Nb, Cr, Mo)–(P, C, B),[29] Co–Fe–(Zr, Hf, Nb)–B[30] and Co–Ta–B[31] systems. It is apparent that the bulk glassy alloys were developed in the sequence beginning with the nonferrous systems, and followed by the Fe- and Co-based alloy systems.[32] Furthermore, it can be seen that the Cu-based bulk glassy alloys defined by Cu contents above 50 at% were the most recently developed,[13,22,23] though other bulk glassy alloys contain Cu as a main solute element.[33,34] When we examine in more detail the features of the alloy components of these bulk glassy alloy systems, the alloy components can be divided into five groups as summarized in Fig. 2. Here ETM and LTM represent the transition metals belonging to the group numbers I to IV and VIII, respectively. The first group consists of ETM–Al–LTM as exemplified by Zr–Al–(Ni, Cu) and Ln–Al–(Ni, Cu). The second group is composed of LTM(Fe), ETM(Zr or Hf) and B and the third group is exemplified by Fe–(Al, Ga)–(P, C, B). The fourth group consists of Mg–Ln–(Ni, Cu) and ETM(Zr, Ti)–Be–(Ni, Cu). It is important to point out that all the alloys belonging to groups I to IV consist of at least three different types of elements with significantly different atomic size mismatches above 12% and negative heats of mixing. The nonequivalent symbols in Fig. 2 represent the difference in the atomic sizes of the constituent elements. Figure 3 summarizes the features of alloy components for stabilization of supercooled liquid and high glass-forming ability of metallic alloys. Accordingly, the newly developed bulk glassy alloys satisfy simultaneously the following three empirical component rules,[3–5] viz., (1) multicomponent consisting of more than three elements, (2) significantly different atomic size mismatches exceeding 12% among the main three constituent elements, and (3) negative heats of mixing among their main elements. In addition, from detailed structural analyses, it has been reported[3–5] that the bulk glassy alloys that conform to the three component rules have a new type of glassy structure with a higher degree of dense random packed atomic configurations, new local atomic configurations and long-range homogeneity with attractive interactions.

Table 1 Typical bulk glassy alloy systems reported to date together with the calendar years when the first paper or patent of each alloy system was published.

1. Nonferrous alloy systems	
Mg–Ln–M	1988
(Ln = lanthanide metal, M=Ni, Cu, Zn)	
Ln–Al–TM	1989
(TM = VI–VIII group transition metal)	
Ln–Ga–TM	1989
Zr–Al–TM	1990
Ti–Zr–TM	1993
Zr–Ti–TM–Be	1993
Zr–(Ti, Nb, Pd)–Al–TM	1995
Pd–Cu–Ni–P	1996
Pd–Ni–Fe–P	1996
Pd–Cu–B–Si	1997
Ti–Ni–Cu–Sn	1998
Cu–(Zr, Hf)–Ti	2001
Cu–(Zr, Hf)–Ti–(Y, Be)	2001
2. Ferrous alloy systems	
Fe–(Al, Ga)–(P, C, B, Si, Ge)	1995
Fe–(Nb, Mo)–(Al, Ga)–(P, B, Si)	1995
Co–(Al, Ga)–(P, B, Si)	1996
Fe–(Zr, Hf, Nb)–B	1996
Co–(Zr, Hf, Nb)–B	1996
Ni–(Zr, Hf, Nb)–B	1996
Fe–Co–Ln–B	1998
Fe–(Nb, Cr, Mo)–(C, B)	1999
Ni–(Nb, Cr, Mo)–(P, B)	1999
Co–Ta–B	1999
Fe–Ga–(P, B)	2000
Ni–Zr–Ti–Sn–Si	2001

When the glassy structure was examined in more detail, it became clear that the atomic configurations differ among the metal-metal type alloys, the metal-metalloid type alloys and the Pd-metalloid type alloys, as illustrated in Fig. 4. For instance, in the metal-metal type glassy alloys, one can see very frequently a unique contrast which is similar to the transverse cross section of an onion as seen in the high resolution TEM image shown in Fig. 5.[35] The onion-like contrast has been explained by computer analysis under the assumption that icosahedral clusters exist in the glassy phase.[36] It has further been confirmed that the density and size of the onion-like contrast regions increase with increasing annealing temperature and/or time.[35] When the diameter of the onion-like contrast region is over 12 nm, it becomes very difficult to discern the reflection spots taken from region A in Fig. 5(b). These reflection spots can be identified as an icosahedral phase whose structure is shown in Fig. 6. These high-resolution TEM images reveal that the glassy structure is composed of icosahedral clusters. Furthermore, the critical size for a transition from icosahedral cluster to icosahedral phase appears to lie around 8 nm.

We also examined the primary crystalline phase which precipitated from the supercooled liquid region for the bulk glassy Zr-based alloys with optimum alloy compositions. Although the bulk glassy alloys in the Zr–Al–Ni–Cu system with a large supercooled liquid region above 80 K were obtained in wide composition ranges, the primary precipitation phase was identified as an fcc-Zr_2Ni phase with a large lat-

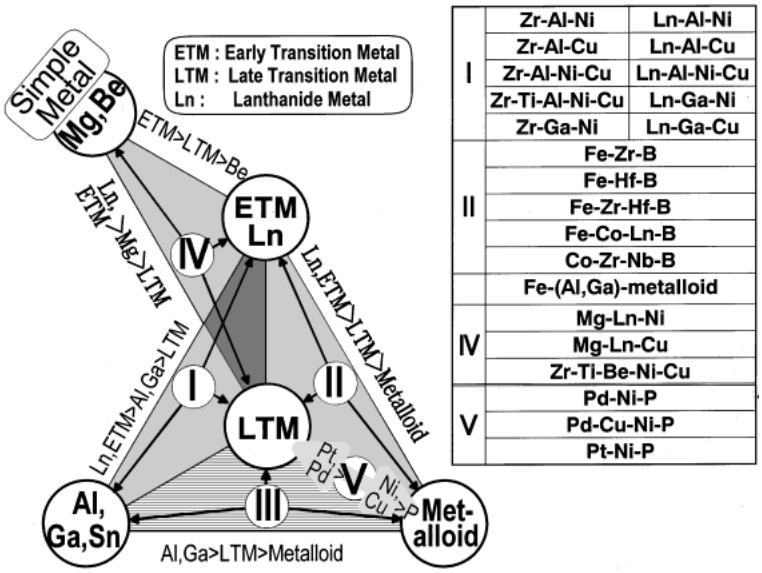

Fig. 2 Feature of alloy components in bulk glassy alloy systems. The alloy components can be divided into five groups.

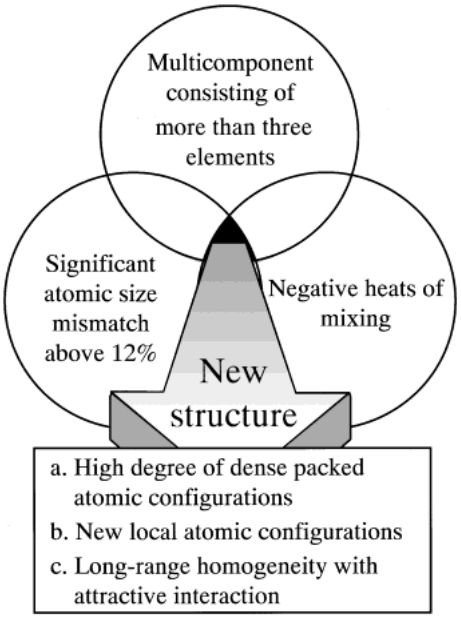

Fig. 3 Features of alloy components for reduced instability of supercooled liquid and high glass-forming ability.

tice parameter of 1.12 nm.[37] This phase is referred to as the "big-cube" phase and is in a metastable state.[38] The unit volume of the big-cube phase consists of 96 atoms and includes slightly distorted icosahedral clusters. The existence of the distorted icosahedral clusters in the primary crystalline phase also indicates the importance of the icosahedral clusters as the fundamental basic unit. This concept is also supported by experimental data from several sources in which the icosahedral phase appears as the primary precipitation phase in Zr-based glassy alloys containing low levels of oxygen as an impurity[39,40] and to which Ag, Pd, Au, Pt, Nb, Ta or V has been added intentionally.[41–44] Here, it is important to point out that the existence of the icosahedral clusters as a main atomic configuration component is consistent with the characteristics of the new glassy structure in the present multi-component alloy systems, *i.e.*, higher degree of dense random packing, new local atomic configurations and long-range homogeneity with attractive interactions.

We also examined the coordination numbers and atomic distances of each atomic pair in the metal-metalloid type Fe–Nb–B[45] and Fe–Ln–B (Ln = lanthanide metal)[46] glassy alloys by anomalous X-ray scattering and ordinary X-ray diffraction methods. Based on the data generated by structural analyses, local atomic configuration models of the Fe-based glassy alloys are shown in Fig. 7. The feature of this type of glassy alloys is the construction of a network atomic configurations consisting of trigonal prisms which are connected with each other through glue atoms comprising Zr, Nb, Ta or lanthanide metal. The Fe-based bulk glassy alloys are characterized in that the primary crystalline phase is a complex fcc-$Fe_{23}B_6$ phase with a large lattice parameter of 1.1 nm and a unit volume consisting of 96 atoms and including icosahedral clusters. As examples, Fig. 8 shows the X-ray diffraction patterns of $Fe_{70}Nb_{10}B_{20}$ and $Fe_{60}Nb_{10}B_{30}$ glassy alloys that have been subjected to annealing so as to precipitate the primary crystalline phase, together with the data on an amorphous $Fe_{80}Nb_{10}B_{10}$ alloy.[45] The diffraction peaks are identified as the $Fe_{23}B_6$ phase for the two glassy alloys and the precipitation phase is independent of B content in the range from 20 to 30 at%B, leading to the formation of the glassy phase. On the other hand, the amorphous $Fe_{80}Nb_{10}B_{10}$ alloy without glass transition before crystallization, has an α-Mn type primary crystalline phase. The characteristics of the primary crystalline phase are nearly identical to those of the Zr-based bulk glassy alloys. Thus we conclude that the main feature of the primary crystalline phase which precipitates from the supercooled liquid in the bulk glassy alloys is independent of the metal-metal and the metal-metalloid types. As is evident from the distinct difference in the atomic configurations between the glassy phase and the primary crystalline phase, the necessity of long-range atomic configurations to construct the primary crystalline phase with a large unit volume from the glassy structure causes retardation of the crystallization reac-

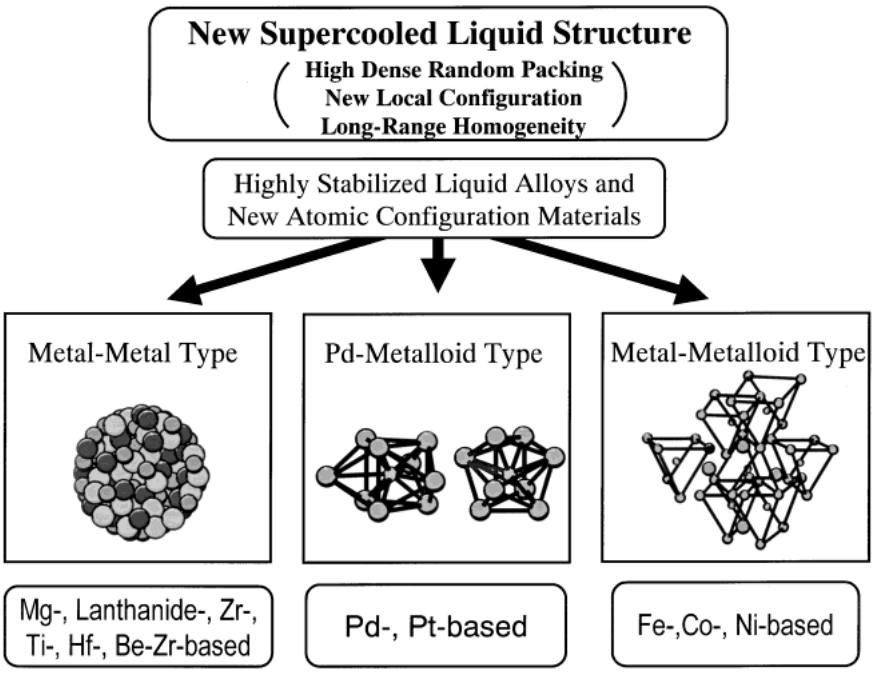

Fig. 4 The details of the unique glassy structure and of the atomic configurations which are different among the metal-metal type alloys, the metal-metalloid type alloys and the Pd-metalloid.

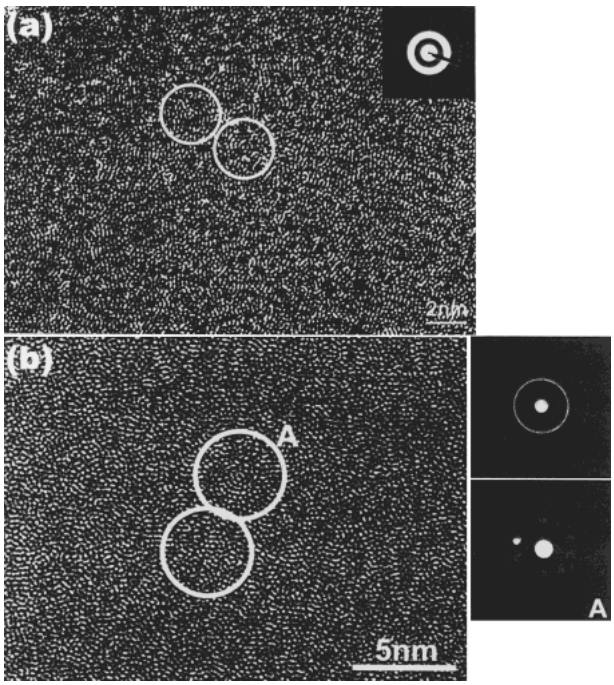

Fig. 5 High-resolution TEM images of $Zr_{70}Pd_{30}$ glassy alloy. (a) as-quenched state. (b) annealed for 120 s at 690 K. The nanobeam diffraction patterns were taken from different areas with a size of approximately 1 nm.

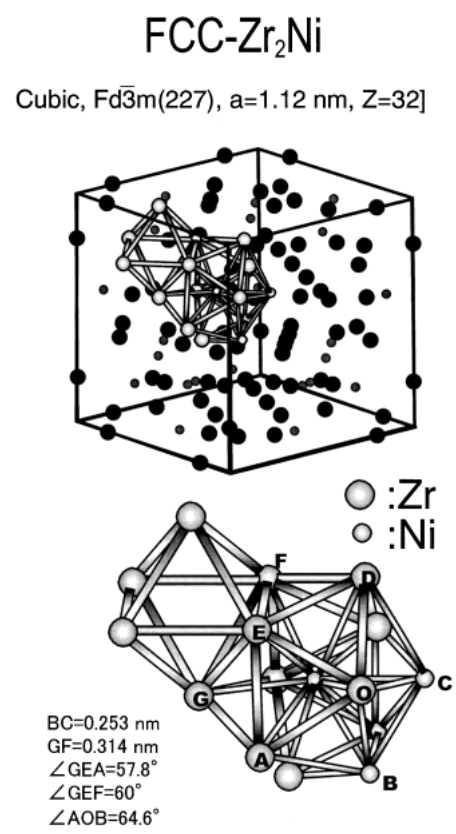

Fig. 6 Atomic structure of a metastable Zr_2Ni phase containing icosahedron in FCC-like unit cell with a large lattice parameter of 1.12 nm.

tion. As described later, this mechanism is concluded to be one of the reasons for the stability of supercooled liquid and the formation of bulk glassy alloys.

It was pointed out that the above-described characteristics of the atomic configurations implied the formation of a new glassy structure with a higher degree of dense random packing. This conjecture is supported by density data[47] obtained using Archimedian method. Table 2 summarizes the densities of typical bulk glassy alloys in as-cast, fully relaxed and crystallized states, together with the difference in densities between the as-cast and annealed states. The difference in the densities is as small as 0.30 to 0.54% which is much smaller than that (about 2%) for ordinary amorphous alloys which require high cooling rates in the order 10^6 K/s for the formation of an amorphous phase. The much smaller difference in den-

Table 2 Densities in as-cast (ρ_a), fully-relaxed ($\rho_{r,a}$) and crystallized (ρ_c) states for typical bulk glassy alloys and the change in density ($\Delta\rho$) by crystallization of their glassy alloys.

	As-cast Glass (ρ_a) [Mg/m^3]	Relaxed Glass ($\rho_{r,a}$) [Mg/m^3]	Crystal (ρ_c) [Mg/m^3]	$\Delta\rho = (\rho_c - \rho_a)/\rho_a$ [%]
$Zr_{60}Al_{10}Cu_{30}$	6.72	—	6.74	0.30
$Zr_{60}Al_{15}Ni_{25}$	6.36	—	6.38	0.31
$Zr_{55}Al_{10}Cu_{30}Ni_5$	6.82	6.38	6.85	0.44
$Pd_{40}Cu_{30}Ni_{10}P_{20}$	9.27	9.28	9.31	0.54
$Zr_{55}Ti_5Al_{10}Cu_{20}Ni_{10}$	6.62	—	6.64	0.30
$Zr_{52.5}Ti_5Al_{12.5}Cu_{20}Ni_{10}$	6.52	—	6.55	0.45

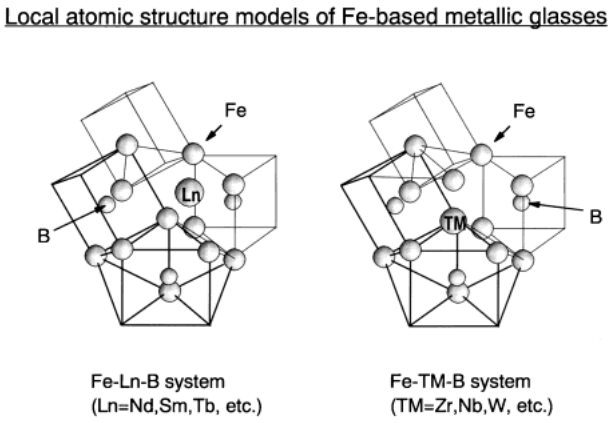

Fig. 7 Local atomic structure models of Fe-based metallic glasses.

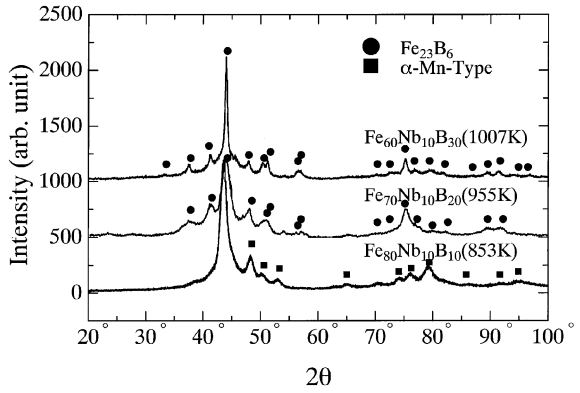

Fig. 8 X-ray diffraction patterns of the $Fe_{70}Nb_{10}B_{20}$ and $Fe_{60}Nb_{10}B_{30}$ glassy alloys subjected to annealing so as to precipitate the primary crystalline phase, together with the data on an amorphous $Fe_{80}Nb_{10}B_{10}$ alloy.

sities indicates clearly that the cast bulk glassy alloys have a higher degree of dense random packed atomic configurations, which is consistent with the above-described results. The smaller difference in the densities also implies that the release of free volume generated by the transition from the supercooled liquid to crystalline phase in the vicinity of the liquid/crystal interface is smaller than that for the ordinary amorphous phase with much larger difference in densities.[48] This leads to the reduction of the interface diffusion of the constituent elements that is thought to be one of the dominant factors promoting crystallization.

Based on the above-described results and discussion, the mechanism for the stabilization of supercooled metallic liquid and the formation of bulk glassy alloys is summarized

Table 3 The mechanisms for the reduced instability of metallic supercooled liquid and the formation of bulk glassy alloys of the Mg-, Ln-, Ti-, Zr- and Hf-based alloys.

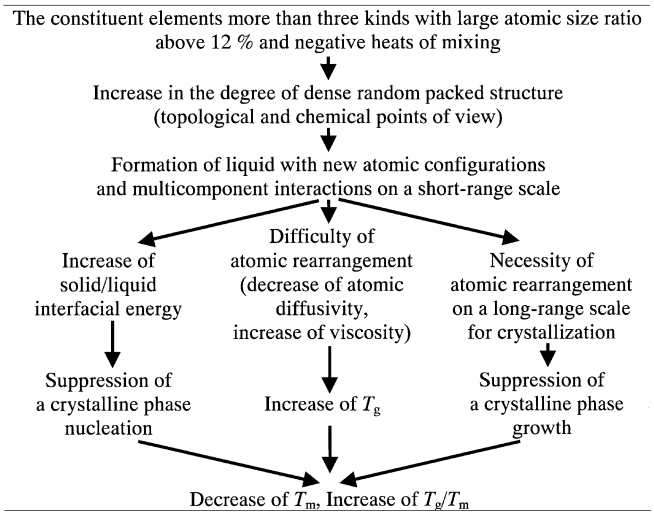

in Table 3.[3–5] The alloys conforming to the three component rules can have unique atomic configurations which are significantly different from those for ordinary amorphous alloys. The unique glassy structure can have high liquid/solid interfacial energy, low atomic diffusivity and require long-range atomic rearrangements for crystallization to proceed, thus producing high stability of supercooled liquid that allow us to form bulk glassy alloys.

3. Stability of Supercooled Liquid

By choosing the above-described multi-component alloys, we can maintain the supercooled liquid state for extended periods reaching several thousandths of a second which are 6 to 8 orders longer than those for conventional crystalline alloys and ordinary amorphous alloys, as illustrated in Fig. 9.[49] As a result, we are able to perform a series of studies on the origins of thermal stability, the structure and properties of the supercooled liquid itself as well as the influence of cleaning and doping on the thermal stability of the supercooled liquid. In addition, we can examine the phase transformation and solidification behavior from the supercooled liquid to glassy or crystalline phase as well as the structure, properties and forming behavior of the resulting bulk glassy alloys. As an example, the experimental results on the stability of the supercooled liquid in the $Pd_{40}Cu_{30}Ni_{10}P_{20}$ glassy alloy are shown

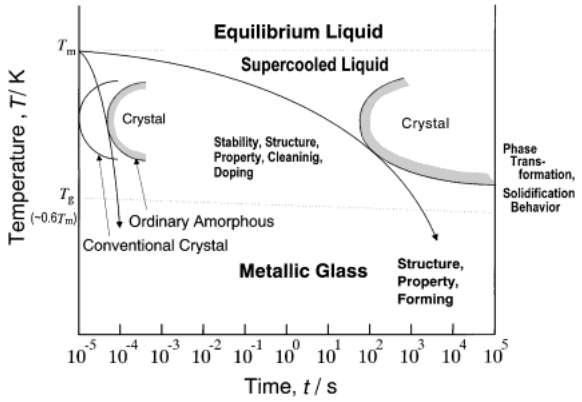

Fig. 9 Schematic diagram showing the high stability of the supercooled liquid state for long periods reaching several thousands of a second.

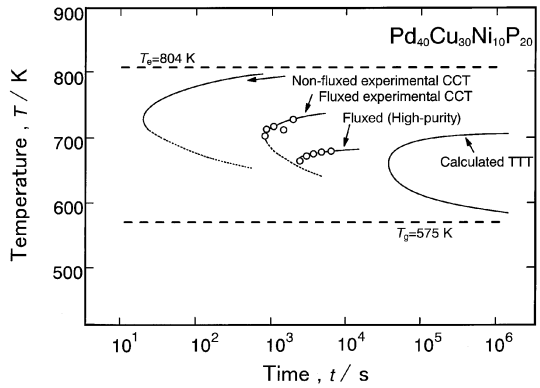

Fig. 10 The experimental results on the stability of the supercooled liquid in the $Pd_{40}Cu_{30}Ni_{10}P_{20}$ glassy alloy.

in Fig. 10.[50] It can be seen that the a supercooled liquid subjected to high purity treatment with B_2O_3 flux could be maintained for a long period of several thousandths of a second even at the nose temperature in the continuous cooling transformation (CCT) curves. It was also found that the incubation time for crystallization at the nose temperature is still 1.5 orders shorter than the homogeneous nucleation state. Achieving the ultimately stabilized supercooled liquid state without heterogeneous nucleation is a challenge that still waits to be overcome. By using the $Pd_{40}Cu_{30}Ni_{10}P_{20}$ alloy that has high stability in the supercooled liquid state, the apparent specific heat of the supercooled liquid can be measured over the whole temperature range.[51] Based on the experimental data, we can determine quantitatively the temperature dependence of enthalpy, entropy and Gibbs free energy for the liquid/crystal transition. The results thus obtained are shown in Fig. 11. As seen in the figure, the Kaufman's temperature is also determined as part of the experimental data. The extremely high stability of the supercooled liquid against crystallization is due to the low free energy for the liquid/crystal transformation.

4. Estimation Methods for Glass-forming Ability and Glass Formation Range

It was shown that the stabilization of supercooled metallic liquid and the high glass-forming ability of alloys could be obtained provided the following three factors were met simul-

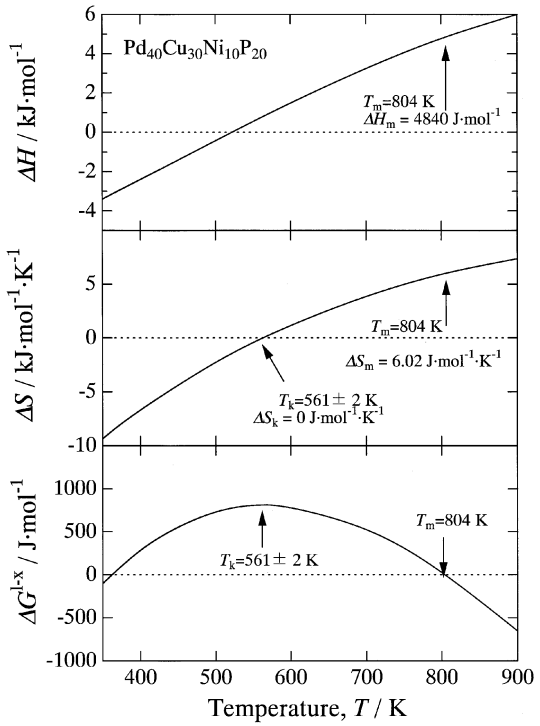

Fig. 11 The temperature dependence of enthalpy, entropy and Gibbs free energy of $Pd_{40}Cu_{30}Ni_{10}P_{20}$ glassy alloy for the transition from the liquid to the crystalline phase.

taneously, viz, (1) multi-component alloy system consisting of more than three elements, (2) significant atomic size mismatches above 12%, and (3) suitable negative heats of mixing. Based on these three component parameters, we have proposed the following relation to estimate the critical cooling rate for glass formation of multi-component alloy systems.[52]

$$R_c = Z\frac{k_B T_m^2}{a^3 \eta_{T=T_m}} \exp\left[f_1 \cdot \left(\frac{\Delta H - T_m \Delta S^{ideal}}{300R} \right) - f_2 \cdot \frac{T_m S_\sigma}{300R} \right]$$

In this relation, the mismatch entropy (S_σ) in the framework of the hard sphere model was used for the parameter of atomic size mismatches among the three main constituent elements. In addition, the mixing enthalpy (ΔH) on the basis of the regular solution approximation was also used for the parameter of negative heats of mixing among their elements. Here, the S_σ[53] and ΔH[54] are presented by the following relations;

$$S_\sigma = k_B \left[\frac{3}{2}(\zeta^2 - 1) y_1 + \frac{3}{2}(\zeta - 1)^2 y_2 - \left\{ \frac{1}{2}(\zeta - 1)(\zeta - 3) + \ln \zeta \right\} (1 - y_3) \right]$$

$$\Delta H = \sum_{\substack{i=1 \\ i \neq j}}^{N} \Omega_{ij} c_i c_j$$

Table 4 summarizes the critical cooling rate (R_c), $Zk_BT_m^2/(a^3\eta)$ term, factors for the reduction of R_c by enthalpy of mixing (ΔH), ideal configuration entropy (ΔS_{ideal}) and mismatch term of entropy (S_σ) for typical amorphous and glassy alloys.[52] It became evident that the R_c values of the glassy and amorphous alloys except Mg–Cu–Y alloy roughly agree

Table 4 Critical cooling rate(R_c), $Zk_BT_m^2/(a^3\eta)$ term, factors for the reduction of R_c by enthalpy of mixing (ΔH), ideal configurational entropy (ΔS^{ideal}) and mismatch term of entropy (S_σ) ($Z^{\Delta H}$, $Z^{\Delta S_{ideal}}$ and Z^{S_σ}) for metallic glasses. $R_c = Zk T_m^2/(a^3\eta) \times Z^{\Delta H} \times Z^{\Delta S_{ideal}} \times Z^{S_\sigma}$.

Alloy	R_c [Ks^{-1}]	$Zk_BT_m^2/(a^3\eta)$ [Ks^{-1}]	$Z^{\Delta H}$	$Z^{\Delta S_{ideal}}$	Z^{S_σ}
Ni	9.1×10^8	9.1×10^8	1	1	1
$Fe_{83}B_{17}$	3.2×10^5	3.9×10^8	1.2×10^{-2}	1.9×10^{-1}	3.6×10^{-1}
$Co_{75}Si_{15}B_{10}$	1.2×10^5	3.8×10^8	6.8×10^{-3}	7.7×10^{-2}	6.1×10^{-1}
$Fe_{79}Si_{10}B_{11}$	2.2×10^5	3.7×10^8	1.2×10^{-2}	9.5×10^{-2}	5.1×10^{-1}
$Fe_{80}P_{13}C_7$	3.8×10^4	1.0×10^8	6.1×10^{-3}	1.4×10^{-1}	4.4×10^{-1}
$Ni_{75}Si_8B_{17}$	4.1×10^4	2.4×10^8	3.7×10^{-3}	8.8×10^{-2}	5.2×10^{-1}
$Pt_{60}Ni_{15}P_{25}$	8.2×10^2	1.2×10^7	1.6×10^{-3}	1.3×10^{-1}	3.3×10^{-1}
$Pd_{82}Si_{18}$	4.4×10^3	1.9×10^7	1.1×10^{-3}	2.8×10^{-1}	7.5×10^{-1}
$Ni_{62.4}Nb_{37.6}$	1.3×10^3	1.2×10^8	2.0×10^{-4}	9.0×10^{-2}	5.9×10^{-1}
$Pd_{77.5}Cu_6Si_{16.5}$	2.6×10^3	1.5×10^7	1.2×10^{-3}	1.8×10^{-1}	8.1×10^{-1}
$Pd_{40}Ni_{40}P_{20}$	7.9×10^2	1.4×10^7	9.4×10^{-4}	8.8×10^{-2}	6.8×10^{-1}
$Pd_{40}Cu_{30}Ni_{10}P_{20}$	1.6×10^{-2}	8.1×10^2	4.9×10^{-4}	7.5×10^{-2}	5.3×10^{-1}
$La_{55}Al_{25}Ni_{20}$	3.1×10^1	1.6×10^8	1.3×10^{-5}	1.8×10^{-1}	8.3×10^{-2}
$Zr_{65}Al_{7.5}Ni_{10}Cu_{17.5}$	3.3×10^2	3.3×10^8	5.8×10^{-5}	5.4×10^{-2}	3.2×10^{-1}
$Zr_{60}Al_{15}Ni_{25}$	1.2×10^1	8.6×10^8	4.2×10^{-7}	6.2×10^{-2}	5.5×10^{-1}
$Fe_{56}Co_7Ni_7Zr_{10}B_{20}$	3.5×10^2	6.9×10^8	1.7×10^{-4}	1.2×10^{-2}	2.5×10^{-1}
$Mg_{65}Cu_{25}Y_{10}$	2.1×10^6	2.3×10^8	1.8×10^{-1}	2.1×10^{-1}	2.4×10^{-1}

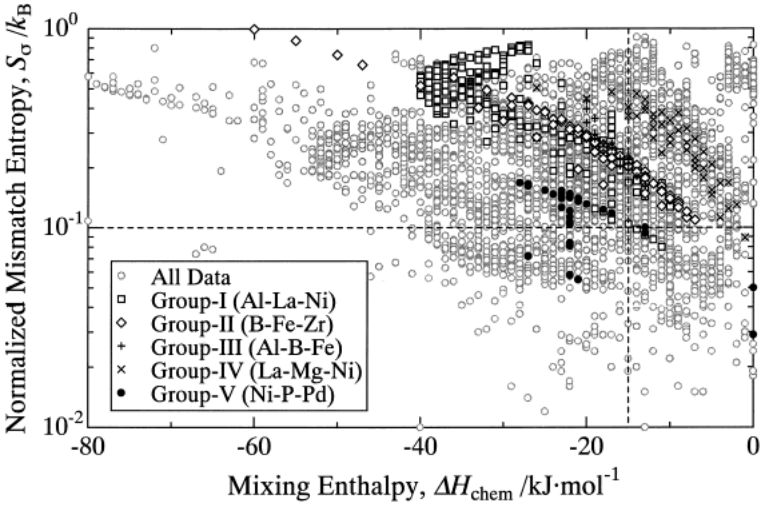

Fig. 12 Relation between ΔH_{chem} and S_σ for the five systems. Two dashed lines are the guidelines showing the critical values for the achievement of high glass-forming ability, obtained by the evaluation of the critical cooling rate for the typical multicomponent metallic glasses.

with the experimental data reported previously. The rough agreement also indicates the importance of the three empirical factors for estimation of glass-forming ability and the effectiveness of the newly proposed relation for estimation of R_c. The disagreement for the Mg–Cu–Y alloy only is thought to result from the small mixing enthalpy values of Mg–Cu and Mg–Y atomic pairs which were estimated by Miedema *et al.*[55] For instance, the heat of mixing is -3 kJ/mol for Mg–Cu pair and -6 kJ/mol for Mg–Y pair. Considering that an amorphous phase is formed in their binary systems, the estimated heats of mixing are reasonably concluded to be smaller than the actual heats of mixing. The importance of the atomic size ratios and heats of mixing among the constituent elements for the formation of bulk glassy alloys is also supported from the statistical data on the mismatch entropy and mixing enthalpy of previous glassy alloy systems. Figure 12 summarizes the relation between the normalized mismatch entropy (S_σ/k_B) and mixing enthalpy (ΔH_{chem}) for glassy alloys reported to date.[56] The S_σ and ΔH_{chem} values of the glassy alloys lie in the vicinity of 0.1 and in the range from -10 to -40 kJ/mol, respectively, though a rather large scattering was observed. In particular, the scattering of the S_σ/k_B values is much smaller than that for the ΔH_{chem}, indicating the importance of the atomic size mismatch ratios. In addition to the estimation of the critical cooling rates for glass formation in multi-component alloy systems, we have also tried to determine the composition range within which a glassy phase is formed in these systems by theoretical computation.[57] In the theoretical computation, the composition range is obtained by satisfying the following criterion: the total enthalpy including the contributions from elasticity, atomic size mismatches, and differing electro-negativities among the constituent elements, must be smaller for the glassy phase than for the crystalline supersaturated solid solution. As examples, the composition

ranges of the glassy phase in Cu–Ni–M (M=Ti, Zr or Hf) ternary alloy systems obtained by the theoretical computation method are shown in Fig. 13,[57] wherein the experimental data are also shown for comparison. Here, the dashed line regions represent the computed composition ranges and the open circles represent the composition of glassy alloys that have been produced experimentally. It is clear that the computed composition ranges agree rather well with the experimental data. This rather good agreement also indicates the importance of the above described three component factors for glass formation. The details of the theoretical calculation have been described in some original papers.

5. Preparation Methods and Maximum Diameters of Bulk Glassy Alloys

The stabilization of supercooled metallic liquid enables us to use various production methods for bulk glassy alloys. The methods can be divided into two types, *i.e.*, solidification and consolidation. As the solidification method, one can list water quenching, low-pressure copper mold casting, high-pressure die casting, arc-melt casting, unidirectional melting, suction casting, squeeze casting, clamp-melt casting and centrifugal casting *etc*.[3–5] In addition, bulk glassy alloys always have a large supercooled liquid region ranging from 50 to 130 K before crystallization and hence some consolidation techniques such as hot pressing, warm extrusion and torsion straining in the supercooled liquid region are also useful for formation of bulk glassy alloys. Table 5 summarizes the maximum thickness and critical cooling rate for bulk glassy alloys. As seen in the table, the maximum thickness is about 10 mm[17] for Ln-based alloys, 12 mm[58] for Mg-based alloys, 30 mm[59] for Zr-based alloys, 5 to 6 mm[60] for Fe-based alloys, 75 mm[15] for Pd-based alloys, 2 mm[31] for Co-based alloys and 5 to 6 mm for Ti-[21] and Cu-[22,23] based alloys. Thus, the glass-forming ability evaluated from the maximum sample diameter decreases in the order of Pd > Zr > Mg > Ln > Ti = Cu = Fe > Ni = Co > Ca systems. It is important to clarify the reason and/or dominant factor for the significant difference in the maximum sample thickness, namely, glass-forming ability among the multi-component alloy systems.

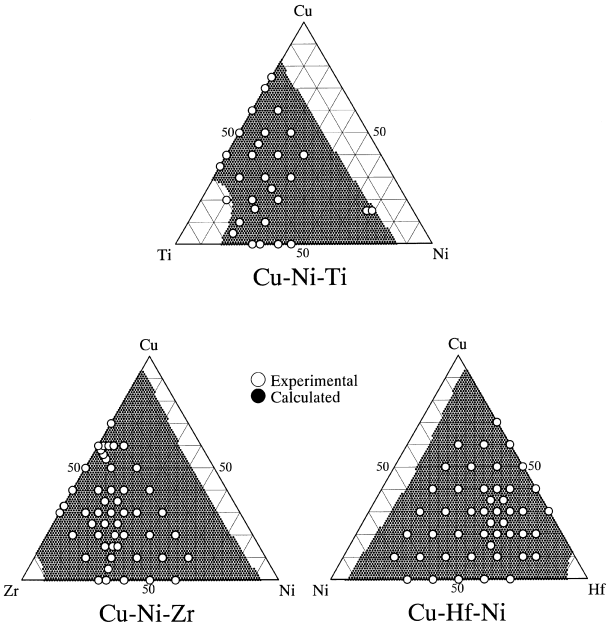

Fig. 13 Experimental and calculated amorphous-forming composition ranges for Cu–Ni–Ti, Cu–Ni–Zr and Cu–Ni–Hf systems.

6. Mechanical Properties–High Strength of New Cu-Based Bulk Glassy Alloys–

Before the general features of the mechanical properties for bulk glassy alloys are presented, it is important to describe the formation and high mechanical strength of new Cu-based bulk glassy alloys. Previously, there had been no data on the formation and properties of Cu-based bulk glassy alloys defined by Cu content exceeding 50 at%Cu.[1–5] Very recently, new Cu-based bulk glassy alloys with high tensile strength were found in very simple alloy systems of Cu–Zr–Ti[13,61] and Cu–Hf–Ti.[61] The addition of small amounts of elements is expected to further increase the glass-forming ability and mechanical strength of these systems, as it has in number of previous cases involving Zr-, Fe-, Mg-, Ni- and Ti-based alloys.[62] Figure 14 shows the shape and outer surface morphology of $Cu_{60}Zr_{29}Ti_9Y_2$ bulk glassy alloys with diameters of 3, 4 and 5 mm produced by copper mold casting.[22] All the rod samples have a smooth surface typical of glassy single phase alloys without crystallinity. The glass transition temperature (T_g), supercooled liquid region ($\Delta T_x = T_x - T_g$) and reduced glass transition temperature (T_g/T_l) of the Cu-based bulk alloys are 700 K, 50 K and 0.63, respectively, and these values are independent of sample diameter up to 5 mm. The use of (T_g/T_l) as reduced glass transition temperature, which is also expressed as (T_g/T_m) in Fig. 1, is based on the recent report[61]

Table 5 Maximum thickness (t_{max}) and critical cooling rate (R_c) of bulk glassy alloys.

Alloy system	t_{max}/mm	R_c/Ks^{-1}
Ln–Al–(Cu, Ni)	≅ 10	≅ 200
Mg–Ln–(Cu, Ni)	≅ 10	≅ 200
Zr–Al–(Cu, Ni)	≅ 30	1–10
Zr–Ti–Al–(Cu, Ni)	≅ 30	1–5
Zr–Ti–(Cu, Ni)–Be	≅ 30	1–5
Fe–(Al, Ga)–(P, C, B, Si)	≅ 3	≅ 400
Pd–Cu–Ni–P	≅ 75	0.1
Fe–(Co, Ni)–(Zr, Hf, Nb)–B	≅ 6	≅ 200
Ti–Ni–Cu–Sn	≅ 6	≅ 200

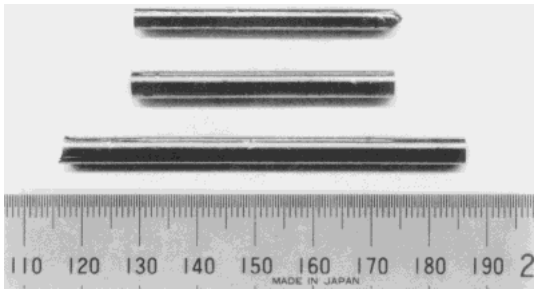

Fig. 14 Shape and outer surface morphology of $Cu_{60}Zr_{29}Ti_9Y_2$ bulk glassy alloys with diameters of 3, 4 and 5 mm produced by copper mold casting.[22]

that glass-forming ability is more closely related to (T_g/T_l) rather than (T_g/T_m). Considering the previous data[63] that the maximum sample diameter of $Cu_{60}Zr_{40}$ binary glassy alloy is less than 1 mm, the multiplication of alloy components by appropriate elements is extremely effective in increasing glass-forming ability and stabilizing supercooled liquid.

Figure 15 shows the stress-elongation curves in compressive and tensile deformation modes for the bulk glassy $Cu_{60}Zr_{30}Ti_{10}$ alloy.[61] Although no distinct plastic elongation is seen in the tensile deformation mode, the Cu-based bulk alloys exhibit a plastic elongation of about 1%. The Young's modulus (E), yield strength (σ_y), elastic elongation (ε_e), tensile fracture strength ($\sigma_{t,f}$), compressive fracture strength ($\sigma_{c,f}$) and compressive fracture elongation ($\varepsilon_{c,f}$) are in the range of 110 to 114 GPa, 1745 to 1785 MPa, 1.5 to 2.0%, 2000 to 2130 MPa, 2000 to 2150 MPa and 3.0 to 3.4%, respectively. It is apparent that the tensile and compressive fracture strength exceed to a significant degree 2000 MPa and are much higher than those for the conventional Zr-based bulk glassy alloys. The fracture in the tensile deformation mode occurs along a maximum shear plane which is declined by 45 to 55 degrees to the direction of applied load and the fracture surface consists mainly of a well-developed vein pattern. The characteristics of the deformation and fracture modes are identical to those for the ordinary bulk glassy alloys with good ductility, being independent of strength level.

With the aim of investigating the mechanism for the high tensile strength of the Cu-based bulk glassy alloys, the relation between the tensile fracture strength ($\sigma_{t,f}$) and T_g or T_l are shown in Fig. 16,[61] where the data on Zr–Al–Ni–Cu bulk glassy alloys are also shown for comparison. A good linear relation between them is apparent. There is a clear tendency for $\sigma_{t,f}$ to increase with increasing T_g or T_l. It is generally known that the T_g and T_l are dominated by the bonding forces among the constituent elements. Consequently, the high mechanical strength of the Cu-based bulk glassy alloys is due to the stronger bonding force among the constituent elements as compared with those for the Zr-based glassy alloys. From the linear relation, the tensile fracture strength is expressed by the following relation, *i.e.*, $\sigma_{t,f} = -3.35 \times 10^3 + 7.47T_g$ and $\sigma_{t,f} = -1.93 \times 10^3 + 3.34T_l$. For a deeper understanding of the strength mechanism, it would be useful to investigate whether or not these relations are satisfied for all bulk glassy alloys reported to date.

Figure 17 summarizes the relation between Young's modulus (E) and tensile fracture strength ($\sigma_{t,f}$) or Vickers hardness (H_v) for typical bulk glassy alloys for which tensile fracture strength values have previously been reported.[61] The data for conventional crystalline alloys are also shown for comparison. It can be seen that the tensile fracture strength and hardness have a linear relation with Young's modulus. A similar linear relation is also evident for ordinary crystalline alloys, but the slope of the linear relation for the bulk glassy alloys is much steeper than that for the ordinary crystalline alloys, indicating clearly that the fundamental mechanical properties of the bulk glassy alloys are significantly different from those for the crystalline alloys. It can also be seen that the scattering of the data from the linear relation is much smaller for the bulk glassy alloys than for the crystalline alloys. The much better linearity is attributed to the formation of an ideally ho-

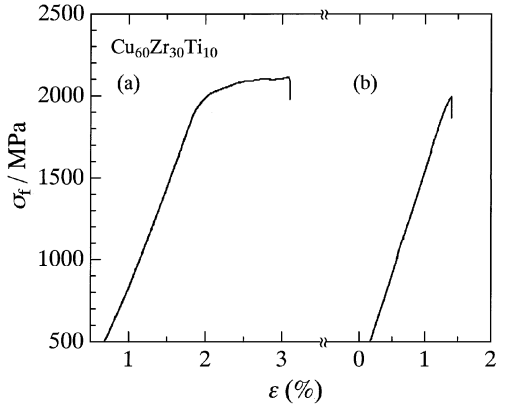

Fig. 15 Stress-elongation curves in (a) compressive and (b) tensile deformation modes for the bulk glassy $Cu_{60}Zr_{30}Ti_{10}$ alloy.

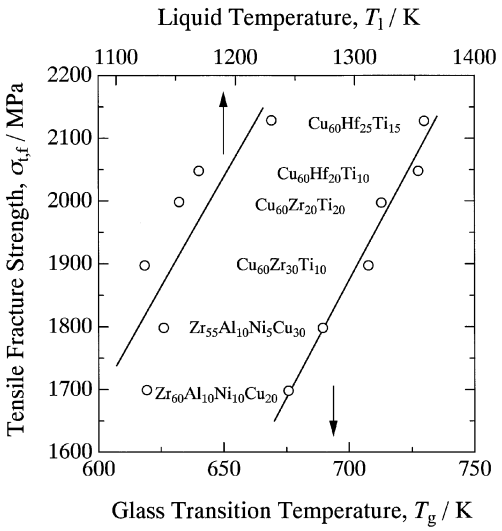

Fig. 16 Relation between the tensile fracture strength ($\sigma_{t,f}$) and T_g or T_l for the high tensile strength Cu-based bulk glassy alloys, together with the data on Zr–Al–Ni–Cu bulk glassy alloys.

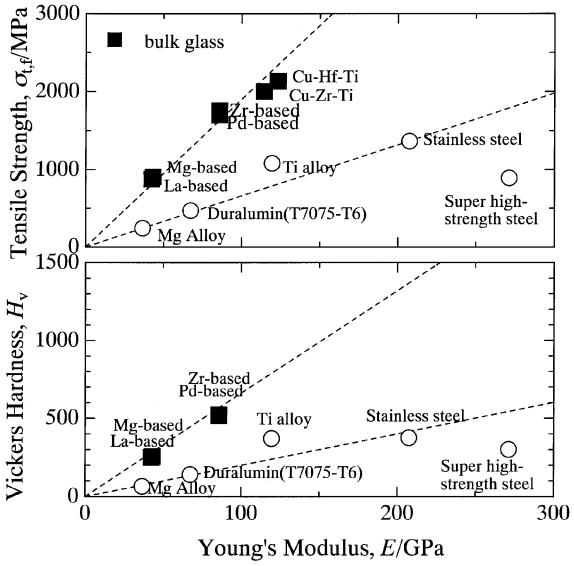

Fig. 17 Relation between Young's modulus (E) and tensile fracture strength ($\sigma_{t,f}$) or Vickers hardness (H_v) for typical bulk glassy alloys for which tensile fracture strength values have previously been reported.

mogenized solid solution over the whole composition range, something which can be regarded as one of the typical characteristics of glassy alloys. From these relations, it is concluded that the mechanical properties for the bulk glassy alloys have the features of much higher tensile strength and much lower Young's modulus. The difference in these values between the glassy and crystalline alloys is as large as 60%. The linear relations are also expressed as follows; $\sigma_{t,f} = 0.02E$, and $H_v = 0.06E/9.8$. The slope value of approximately 0.02 corresponds to an elastic strain limit and hence the glassy alloys can have a much larger elastic strain. The significant difference in the mechanical properties is thought to be a reflection of the difference in the deformation and fracture mechanisms between bulk glassy and crystalline alloys.[61] Finally, it is important to point out that the Cu-based bulk glassy alloys have the highest tensile strength among all bulk glassy alloys and the strength level is about two times higher than the highest tensile strength of conventional Cu-based crystalline alloys.

In addition to the high static mechanical strength, the Zr-based bulk glassy alloys exhibit high Charpy impact fracture energies ranging from 110 to 140 kJ/m^2 and high fracture toughness of 60 to 70 MPa $\cdot \sqrt{m}$.[64] Furthermore, the fatigue endurance limit defined by the ratio of maximum applied stress (σ_{max}) to tensile fracture strength ($\sigma_{t,f}$) has been reported to be about 0.25 for the $Zr_{65}Al_{10}Ni_{10}Cu_{15}$ and $Pd_{40}Cu_{30}Ni_{10}P_{20}$ bulk glassy alloys under the three-point bending and the rotating-beam bending fatigue test conditions at room temperature.[65] The fatigue limit is nearly the same as those for ordinary crystalline alloys. Considering that the tensile fracture strength of the bulk glassy alloys is about double that of the crystalline alloys, the fatigue endurance stress level is also much higher for the bulk glassy alloys. The propagation velocity of fatigue cracks (da/dn) under the rotating-beam bending load for the $Zr_{60}Al_{10}Ni_{10}Cu_{20}$ bulk glassy alloy is shown as a function of the ratio of effective stress intensity factor to Young's modulus ($\Delta K_{eff}/E$) in Fig. 18.[66] A good linear relation is evident between these properties, indicating that the fatigue crack propagation velocity can be estimated from the values of ΔK_{eff} and E. Furthermore, the crack propagation behavior is in agreement with ordinary carbon steels and appears to be independent of structure. Consequently, it may be concluded that the difference in glassy and crystalline structures does not play a dominant role in the propagation velocity of fatigue cracks, though the deformation and fracture behavior under a uni-axial applied load is significantly different from those for crystalline alloys.

Because of their good mechanical properties and high reliability, Zr-based bulk glassy alloys have already been used in the manufacture of sporting goods[67,68] and Pd-based alloy systems as die and electrode materials.[64] Furthermore, success in creating new cost effective Cu-based bulk glassy alloys with much higher tensile strength and good ductility[61] is promising for their future application as high-strength materials.

7. Soft Magnetic Bulk Glassy Alloys in Fe- and Co-based Systems

Since the first synthesis of Fe-based bulk glassy alloys in an Fe–(Al, Ga)–P–C–B system in 1995,[11] a number of bulk

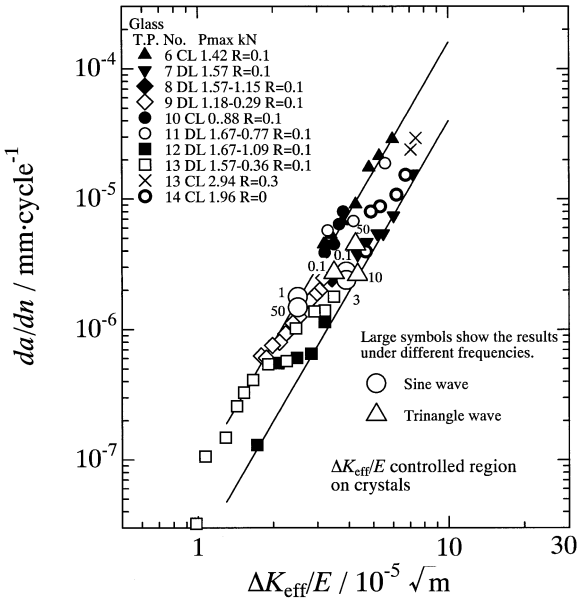

Fig. 18 Propagation velocity of fatigue cracks (da/dn) under the rotating-beam bending load for the $Zr_{60}Al_{10}Ni_{10}Cu_{20}$ bulk glassy alloy as a function of the ratio of effective stress intensity factor to Young's modulus ($\Delta K_{eff}/E$).

Table 6 Alloy systems in which bulk glassy Fe- and Co-based alloys with diameters above 1 mm are formed by the copper mold casting method.[69]

System	Years
Fe–(Al, Ga)–(P, C, B, Si, Ge)	1995
Fe–(Nb, Mo)–(Al, Ga)–(P, B, Si)	1995
Co–(Al, Ga)–(P, B, Si)	1996
Fe–(Zr, Hf, Nb)–B	1996
Co–Fe–(Zr, Hf, Nb)–B	1996
Fe–Co–Ln–B	1998
Fe–(Nb, Cr, Mo)–(P, C, B)	1999

glassy alloys have been developed over the last five years. Table 6 summarizes the alloy systems in which bulk glassy Fe- and Co-based alloys with diameters above 1 mm have been formed by the copper mold casting method.[69] As typical Fe-based bulk glassy alloys, one can see the following four basic types consisting of Fe–(Al and/or Ga)–P–C–B,[70] Fe–(Zr, Hf, Nb and/or Ta)–B,[71] Fe–Co–Ln–B[72] and Fe–(Cr, Mo and/or Nb)–B–C.[73] As is the case for bulk glassy alloys in the other alloy systems, the glass-forming ability of these Fe-based alloys is expected to be improved by the addition of a small amount of elements. The maximum diameter of the Fe-based bulk glassy alloys has been reported to reach 5 to 6 mm for the Fe–(Zr, Hf, Nb)–(Cr, Mo, W)–B based system.[60]

Table 7 summarizes the advantages and disadvantages for soft magnetic properties, comparing the soft magnetic properties of Fe- and Co-based amorphous alloys with a maximum sample thickness of about 30 μm.[74] Advantages to note are (1) much higher glass-forming ability leading to the formation of thicker sheets and plates, larger diameter wire and thick ring, (2) higher electrical resistivity of 220 to 250 μΩcm at room temperature, (3) more homogeneous glassy structure without clusters for crystal nucleation, (4) appearance of a large supercooled liquid region before crystallization, (5) lower coercive force of 0.2 to 4 A/m, (6) higher initial perme-

Table 7 Advantages and disadvantages of soft magnetic properties, comparing the soft magnetic properties of Fe- and Co-based amorphous alloys with a maximum sample thickness of about 30 μm.[74)]

Advantages	Disadvantages
(1) much higher glass-forming ability	(1) higher materials cost
(2) higher electrical resistivity	(2) lower saturated magnetic flux density
(3) more homogeneous glassy structure	
(4) appearance of a large supercooled liquid region	
(5) lower coercive force	
(6) higher initial permeability	
(7) intentional arrangement of domain wall structure	
(8) better high-frequency permeability	
(9) good micro-forming ability	
(10) warm consolidation into a highly dense bulk form	

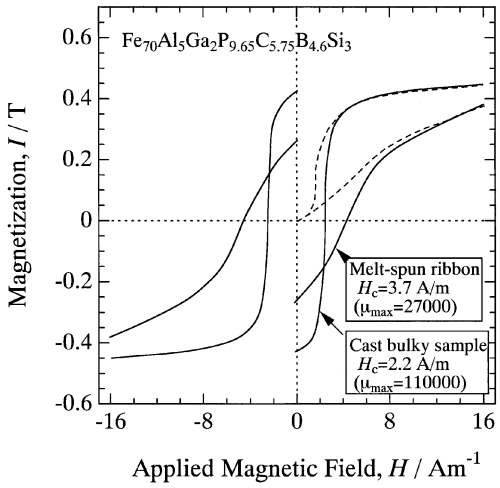

Fig. 19 I-H hysteresis loop of the cast ring-shape Fe-based glassy alloy,[75)] together with the data on the similar ring-shape alloy made by stacking the melt-spun ribbons with a thickness of about 0.02 mm.

ability, (7) intentional arrangement of domain wall structure caused by the control of casting and/or cooling conditions, (8) better high-frequency permeability, (9) good micro-forming ability in the supercooled liquid region, and (10) warm consolidation into a highly dense bulk form. On the other hand, the disadvantages are (1) higher materials cost due to the necessity of using special solute elements to obtain an increase in glass-forming ability, and (2) lower saturated magnetic flux density due to the addition of larger amounts of solute elements. In particular, the lower saturated magnetic flux density for soft magnetic glassy alloys is a serious obstacle to future use in power transformers. Consequently, a great deal of time and effort have been devoted to increasing the saturated magnetic flux density, though there exists a trade-off relation between the decrease in the solute contents for an increase in saturated magnetic flux density and the increase in the solute content for an increase in glass-forming ability.

Here, some of the evidence supporting the advantages of soft magnetic glassy alloys will be cited. Figure 19 shows the I-H hysteresis loop of the cast ring-shape Fe-based glassy

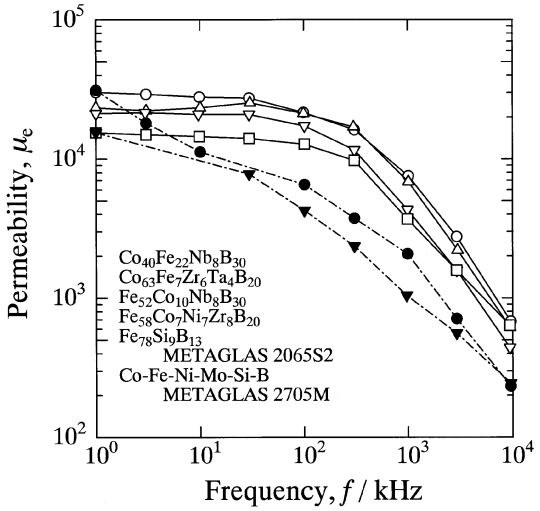

Fig. 20 High frequency permeability of Co–Fe–Zr–B and Co–Fe–Zr–(Nb or Ta)–B glassy alloys annealed for 600 s at temperatures between T_c and T_g.

alloy,[75)] together with the data on the similar ring-shaped alloy made by stacking the melt-spun ribbons with a thickness of about 0.02 mm. The ring sample has a thickness of 1 mm, an outer diameter of 10 mm and an inner diameter of 6 mm. It can be seen that the bulk-ring shape alloy has a lower coercive force of 2.2 A/m and a much higher initial maximum permeability of 110000 even in the as-cast state. Based on the observation results of domain wall structure for these samples, it has been conjectured that the much better soft magnetic properties for the cast ring-shape alloy are due to the well-arrayed domain wall structure in which the domain wall is arrayed in the circumferential direction. It was demonstrated that subsequent annealing treatment of the ring-shape sample caused a further increase in initial permeability to 180000 accompanied by a decrease in coercive force to 1.0 A/m. As is the case for initial permeability, the soft magnetic glassy alloys exhibit much better high-frequency permeability such as 6000 to 7000 at 1 MHz, as shown for Co–Fe–Nb–B and Co–Fe–Zr–Ta–B alloys in Fig. 20.[76)] It can be seen that the frequency permeability of the glassy-type alloy exceeds those for Fe- and Co-based amorphous alloys over the whole frequency range. The good high-frequency permeability is due to the combination of low coercive force resulting from the homogeneous glassy structure and low eddy current loss resulting from high electrical resistivity. Further increases in electrical resistivity and decreases in the sample thickness are expected to bring about even better high-frequency permeability characteristics. Although the ferromagnetic glassy alloy has the disadvantage of lower saturated magnetic flux density, the disadvantage has been significantly suppressed by fine adjustment of alloy components. Table 8 summarizes soft magnetic properties of Fe–Co–Ln–B (Ln = lanthanide metals) glassy alloys, together with thermal stability data.[72)] The best combination of 1.53 T for saturated magnetic flux density (I_s), 4.03 A/m for coercive force (H_c), 12700 for effective permeability (μ_e) at 1 kHz and 23.5×10^6 for saturated magnetostriction (λ_s) is obtained for $Fe_{71.5}Nd_3Dy_{0.5}B_{25}$ glassy alloy subjected to annealing for 600 s at 773 K. The I_s value is comparable to those for conventional Fe-based amorphous alloys. In addi-

Table 8 Thermal stability and magnetic properties of $Fe_{62}Co_{9.5}Ln_{3.5}B_{25}$ glassy alloys, together with the thermal stability data.[72)]

Composition (at%)	Thermal stability			Magnetic properties			
	T_g/K	T_x/K	ΔT_x/K	I_s/T	H_c/Am^{-1}	$\lambda_s/10^{-6}$	μ_e (at 1 kHz)
$Fe_{62}Co_{9.5}Pr_{3.5}B_{25}$	833	884	51	1.36	3.7	22	10600
$Fe_{62}Co_{9.5}Nd_3Dy_{0.5}B_{25}$	844	900	56	1.41	2.6	24	12000
$Fe_{62}Co_{9.5}Sm_{3.5}B_{25}$	841	893	52	1.35	3.8	23	11700
$Fe_{62}Co_{9.5}Gd_{3.5}B_{25}$	844	907	63	1.41	1.9	24	11000
$Fe_{62}Co_{9.5}Dy_{3.5}B_{25}$	856	914	58	1.43	3.0	19	8300
$Fe_{62}Co_{9.5}Tb_{3.5}B_{25}$	842	903	61	1.36	3.1	27	12500
$Fe_{62}Co_{9.5}Er_{3.5}B_{25}$	830	884	54	1.38	1.0	32	8900

tion, the Fe-based alloy also has a distinct glass transition and a large supercooled liquid region of 56 K before crystallization. Consequently, it is very likely that further improvements to the soft magnetic properties will allow the practical use of glassy-type alloys as soft magnetic materials.

8. Corrosion Resistant Bulk Glassy Alloys

Since 1995, Fe-based bulk glassy alloys have been developed in various alloy systems in which the features of the alloy components have been divided into the above-described four types. It has been reported that good soft magnetic properties are obtainable for three types of alloys, *i.e.*, Fe–(Al or Ga)–P–C–B,[70)] Fe–(Zr, Hf, Nb, Ta)–B[71)] and Fe–Co–Ln–B.[72)] This is reminiscent of another Fe-based bulk glassy alloy, the Fe–(Cr, Mo)–(C, B, P) system.[73)] The largest supercooled liquid region of 58 K as well as high reduced glass transition temperature above 0.60 is obtained in the vicinity of $Fe_{43}Cr_{16}Mo_{16}C_{15}B_{10}$, and a suitable choice of alloy composition has enabled us to form bulk glassy alloys with diameters up to about 3 mm.[77)] Figure 21 shows the relation between anodic current density and potential in 6N HCl at 298 K for glassy $Fe_{43}Cr_{16}Mo_{16}C_{15}B_{10}$ and $Fe_{43}Cr_{16}Mo_{16}C_{10}B_5P_{10}$ alloys of 2.7 mm and 2.2 mm in diameter, respectively.[77)] Even under this extremely severe corrosive environment, these bulk glassy alloys exhibit passive behavior, indicating that they have high corrosion resistance. The resistance is considerably higher for the P-containing bulk alloy. We have also confirmed that the corrosion loss in 6N HCl at 298 K is about 10^5 times larger for type 304 stainless steel than for the P-containing bulk glassy alloy.[77)] These results indicate that the corrosion resistance is good enough to use the Fe-based bulk glassy alloys as practical corrosion resistant materials.

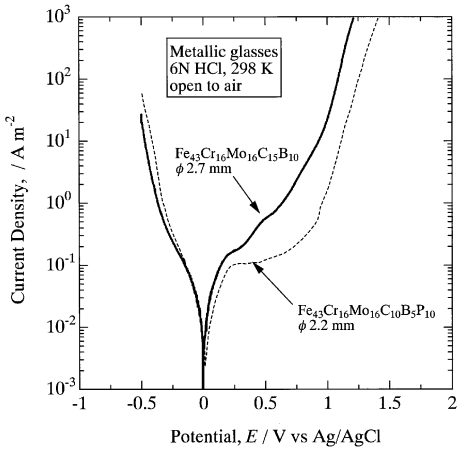

Fig. 21 Potentiodynamic polarization curves of $Fe_{43}Cr_{16}Mo_{16}C_{15}B_{10}$ and $Fe_{43}Cr_{16}Mo_{16}C_{10}B_5P_{10}$ bulk metallic glasses in 6N HCl solution open to air at 298 K.

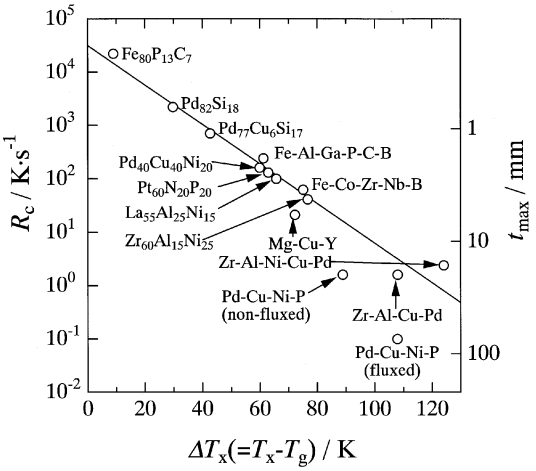

Fig. 22 Relations among the supercooled liquid region before crystallization, $\Delta T_x(= T_x - T_g)$, R_c and t_{max} for various bulk glassy alloys.

9. Working and Welding in the Supercooled Liquid Region

It has generally been recognized that a large supercooled liquid region is observed for all bulk glassy alloys.[3–5)] Figure 22 shows the relations among the supercooled liquid region before crystallization, $\Delta T_x(= T_x - T_g)$, R_c and t_{max} for various bulk glassy alloys.[78)] It is clear that a strong correlation exists and the increase in ΔT_x causes a decrease in R_c and an increase in t_{max}, though the correlation is weaker when compared with the relation among T_g/T_m, R_c and t_{max} shown in Fig. 1. In any event, all the bulk glassy alloys have a supercooled liquid region with a temperature interval ranging from 40 to 130 K. Figure 23 shows the relation between stress and strain rate at different temperatures including the supercooled liquid region for $Zr_{65}Al_{10}Ni_{10}Cu_{15}$ and $La_{55}Al_{25}Ni_{20}$ glassy alloys.[79,80)] Although the viscosity in the temperature range below T_g decreases almost linearly with increasing strain rate, the viscosity in the supercooled liquid region remains constant in the low strain rate range, indicating that controlling deformation temperature and strain rate in the supercooled liquid region generate an ideal Newtonian flow for bulk glassy alloys. Under the deformation condition where Newtonian

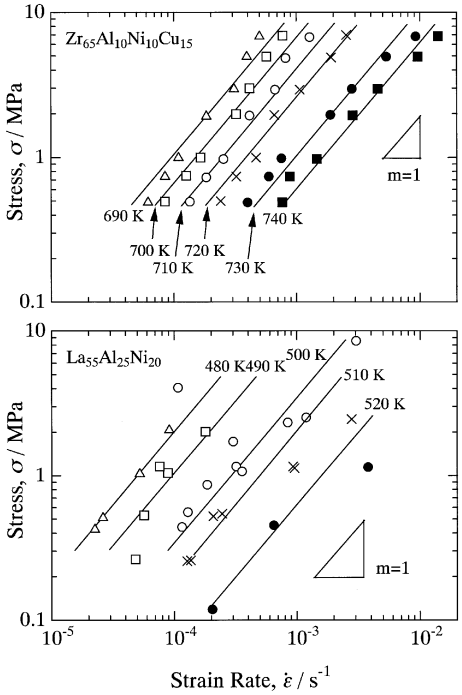

Fig. 23 Relation between stress and strain rate at different temperatures including the supercooled liquid region for $Zr_{65}Al_{10}Ni_{10}Cu_{15}$ and $La_{55}Al_{20}Ni_{25}$ glassy alloys.

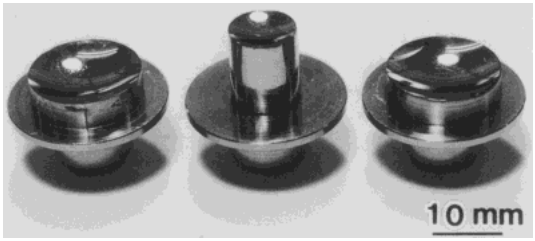

Fig. 24 Optical precision parts of a bulk glassy $Zr_{65}Al_{10}Ni_5Cu_{30}$ alloy prepared by die forging in the supercooled liquid.

flow is obtained, we have also shown that a linear relation exists between true stress and strain rate and the slope corresponding to the strain rate sensitivity exponent (m-value) is found to be 1.0.[81] Thus, ideal superplastic behavior is achieved by controlling deformation condition in the supercooled liquid region. By utilizing the ideal superplasticity, we can obtain an extremely large elongation of 1.5×10^6%, a very smooth outer surface on a nanoscale together with welding and joining between glassy alloy and stainless steel, as demonstrated in Fig. 24.[82] The precise forming can also be performed in the supercooled liquid region for the glassy alloys. As a result, we can obtain small glassy gears with small diameters up to 0.2 mm and a thickness of 0.01 mm[83] as well as various imprinted patterns on micrometer and nanometer scales.[84] As examples, some imprinted patterns formed on the outer surface of Pd-based glassy alloys are shown in Fig. 25.[84] Such imprinted patterns are also important for future application in the recording materials field. In addition to the above-described micro-forming treatments, it has been recognized that the bulk glassy alloy can keep a smooth outer surface on a fine scale of 2 to 3 nm even in the mechanically cut state.[85]

Table 9 Present and future application fields for bulk glassy alloys.

Fundamental characteristic	Application field
High strength	Machinery structural materials$^{\triangle}$
High hardness	Optical precision materials*
High fracture toughness	Die materials$^{\triangle}$
High impact fracture energy	Tool materials
High fatigue strength	Cutting materials$^{\triangle}$
High elastic energy	Electrode materials$^{\#}$
High corrosion resistance	Corrosion resistant materials
High wear resistance	Hydrogen storage materials
High viscous flowability	Ornamental materials$^{\triangle}$
High reflection ratio	Composite materials
Good soft magnetism	Writing appliance materials*
High frequency permeability	Sporting goods materials$^{\#}$
High magnetostriction	Bonding materials
Efficient electrode (Chlorine gas)	Soft magnetic materials$^{\triangle}$
High hydrogen storage	High magnetostrictive materials
	#: Practical use, ∗: Use in company
	△: Trial for practical use

10. Application Fields and Future Trends

Table 9 summarizes present and future application for the bulk glassy alloys. As described above, the bulk glassy alloys have various unique properties which are not obtainable in conventional crystalline alloys, in addition to the great advantages of direct formation of bulk alloys from liquid and the easy formation of variety of shapes while in the supercooled liquid region. Because of these unique advantages, the bulk glassy alloys have already been used as die materials (Pd–Cu–Ni–P alloys), sporting goods materials (Zr–Al–Ni–Cu alloys) and electrode materials (Pd–Cu–Si–P alloys). Furthermore, Fe-based glassy alloys have reached the final stage of their development for application as soft magnetic materials for common mode choke coils. Success in this area will soon result in bulk glassy alloys becoming far more important in engineering.[3–5]

Figure 26 summarizes new materials in science and technology produced from stabilized supercooled liquid.[49] The supercooled liquid has enabled us to study the formation, structure, properties, viscous flow forming and direct production techniques for bulk glassy alloys. In addition, we are now able to purposefully alter the properties of bulk glassy alloys, using the three empirical component "rules" for the stabilization of supercooled liquid. It has been confirmed when the alloy components are intentionally changed so as to deviate from the "rules", the resulting structure changes to bulk glassy alloys containing nanoscale crystalline[86] or quasicrystalline[87] particles and to a crystalline supersaturated solid solution[88] with nanograin sizes. It has also been shown that the change into a nanostructure improves various characteristics. Therefore, in the near future, studies on stabilized supercooled liquid and the resulting bulk alloys with a glassy single phase, nanocrystalline phase, nanoquasicrystalline phase and supersaturated solid solution with nanoscale grain size will become more and more significant for basic science and engineering applications.

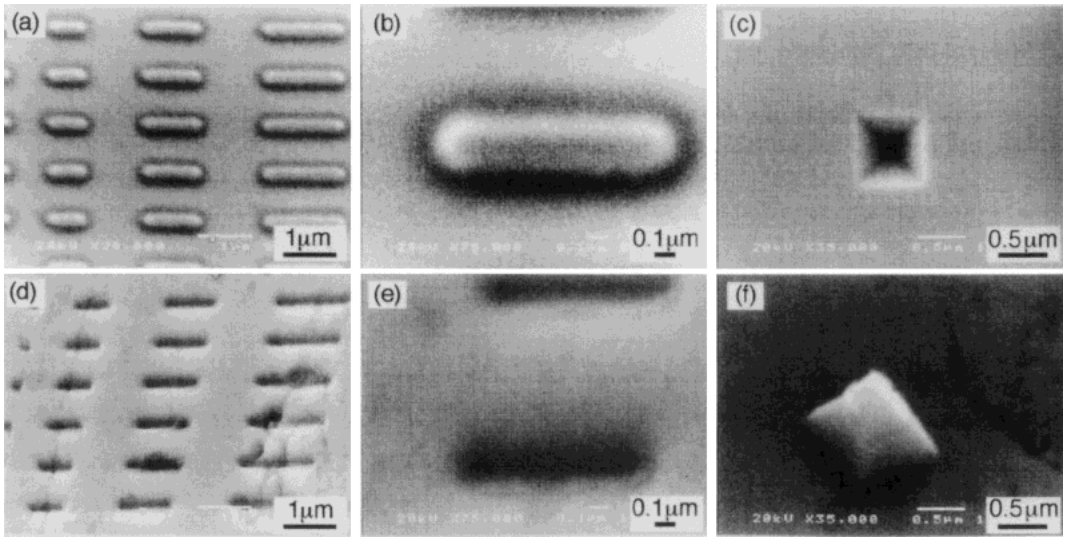

Fig. 25 SEM micrographs of fabricated micro-dies and nano-formed specimens of $Pd_{40}Cu_{30}Ni_{10}P_{20}$ amorphous alloy. SEM microphotographs of (a,b) nanometer-sized die and (d,e) imprinted specimen. The width of each pit pattern is 200 nm. SEM microphotographs of (c) nanometer-sized die and (f) deformed-pyramid of 500 nm in base length. Applied mean stress $\sigma_m = 10$ MPa. Maximum forming temperature $T_{w.max} = 640$ K. Forming time $t_w = 1$ ksec.

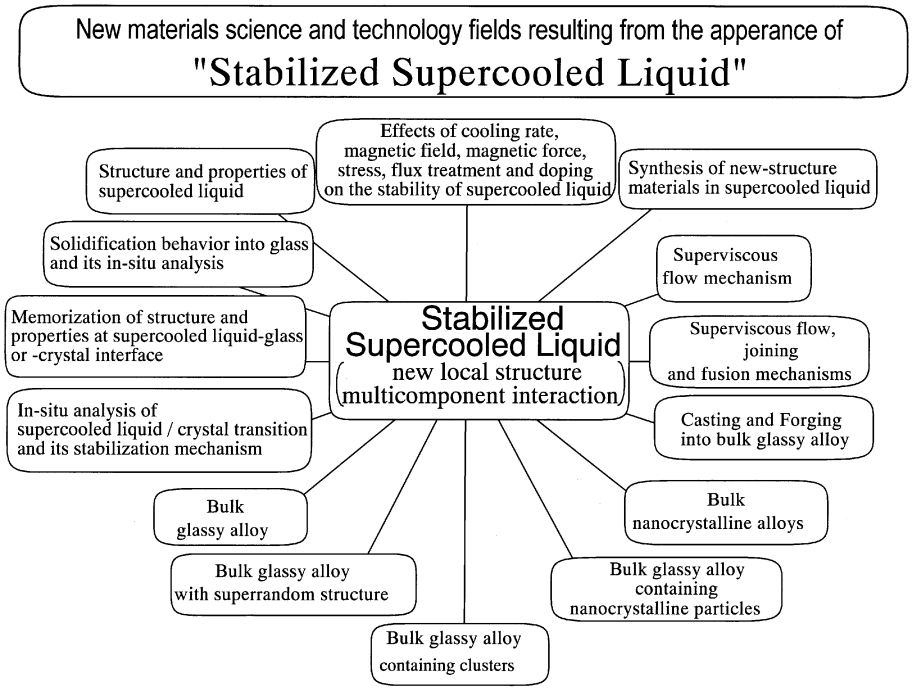

Fig. 26 New materials resulting from stabilized supercooled liquid for application in the fields of science and technology.[49)]

REFERENCES

1) H. S. Chen: Rep. Prog. Phys. **43** (1980) 353–432.
2) R. W. Cahn: *Rapidly Solidified Alloys*, ed. by H. H. Liebermann, (Marcel Dekker, New York, 1993) pp. 1–788.
3) A. Inoue: Mater. Trans., JIM **36** (1995) 866–875.
4) A. Inoue: Acta Mater. **48** (2000) 279–306.
5) A. Inoue: Mater. Sci. Eng. **A304–306** (2001) 1–10.
6) A. Inoue, T. Zhang and T. Masumoto: Mater. Trans., JIM **30** (1989) 965–972.
7) A. Inoue, K. Ohtera, K. Kita and T. Masumoto: Jpn. J. Appl. Phys. **27** (1988) L2248–L2251.
8) A. Inoue, T. Zhang and T. Masumoto: Mater. Trans., JIM **31** (1990) 177–183.
9) A. Peker and W. L. Johnson: Appl. Phys. Lett. **63** (1993) 2342–2344.
10) A. Inoue, N. Nishiyama, K. Amiya, T. Zhang and T. Masumoto: Mater. Lett. **19** (1994) 131–135.
11) A. Inoue and J. S. Gook: Mater. Trans., JIM **36** (1995) 1180–1183.
12) A. Inoue, N. Nishiyama and T. Matsuda: Mater. Trans., JIM **37** (1996) 181–184.
13) A. Inoue, W. Zhang, T. Zhang and K. Kurosaka: Mater. Trans. **42** (2001) 1149–1151.
14) N. Nishiyama and A. Inoue: Appl. Phys. Lett., **80** (2002) 568–570.
15) A. Inoue, N. Nishiyama and H. M. Kimura: Mater. Trans., JIM **38** (1997) 179–183.
16) A. Inoue, T. Nakamura, N. Nishiyama and T. Masumoto: Mater. Trans., JIM **33** (1992) 937–945.
17) A. Inoue, T. Nakamura, T. Sugita, T. Zhang and T. Masumoto: Mater. Trans., JIM **34** (1993) 351–358.
18) T. Zhang, A. Inoue and T. Masumoto: Mater. Trans., JIM **32** (1991) 1005–1010.
19) A. Inoue, T. Shibata and T. Zhang: Mater. Trans., JIM **36** (1995) 1420–

1426.
20) Y. He, T. D. Shen and R. B. Schwarz: Metall. Mater. Trans. A **29** (1998) 1795–1804.
21) A. Inoue: Mater. Sci. Forum **312–314** (1999) 307–314.
22) T. Zhang, K. Kurosaka and A. Inoue: Mater. Trans. **42** (2001) 2042–2045.
23) A. Inoue, T. Zhang and K. Kurosaka and W. Zhang: Mater. Trans. **42** (2001) 1800–1804.
24) A. Inoue, H. M. Kimura and G. S. Gook: Mater. Trans., JIM **37** (1996) 32–38.
25) B. Shen and A. Inoue: Mater. Trans **41** (2000) 873–876.
26) T. D. Shen and R. D. Schwarz: Appl. Phys. Lett. **75** (1999) 49–51.
27) A. Inoue, T. Zhang, H. Koshiba and A. Makino: J. Appl. Phys. **83** (1998) 6326–6328.
28) W. Zhang and A. Inoue: Mater. Trans., JIM **40** (1999) 78–81.
29) S. Pang, T. Zhang, K. Asami and A. Inoue: Mater. Trans. **42** (2001) 376–379.
30) T. Itoi and A. Inoue: Mater. Trans., JIM **41** (2000) 1256–1262.
31) B. L. Shen, H. Koshiba, A. Inoue, H. M. Kimura and T. Mizushima: Mater. Trans., JIM **41** (2001) 2136–2139.
32) A. Inoue, A. Takeuchi and T. Zhang: Metall. Mater. Trans. A **29** (1998) 1779–1793.
33) H. Choi-Yim, R. Busch and R. W. L. Johnson: J. Appl. Phys. **83** (1998) 7993–7997.
34) A. Inoue, W. Zhang, T. Zhang and K. Kurosaka: J. Mater. Res. **16** (2001) 2836–2844.
35) J. Saida, M. Matsushita and A. Inoue: Appl. Phys. Lett. **79** (2001) 412–414.
36) T. Takagi, T. Ohkubo, Y. Hirotsu, B. S. Murty, K. Hoho and D. Shindo: Appl. Phys. Lett. **79** (2001) 485–487.
37) C. Li, J. Saida and A. Inoue: Mater. Trans., JIM **41** (2000) 1521–1525.
38) U. Koster, J. Meinhardt, S. Roos and A. Rudiger: Mater. Sci. Forum **225** (1996) 311–316.
39) J. Eckert, N. Mattern, M. Zinkevitch and M. Seidel: Mater. Trans., JIM **39** (1998) 623–632.
40) B. S. Murty, D. H. Ping, K. Hono and A. Inoue: Mater. Sci. Eng. A **304** (2001) 706–709.
41) M. W. Chen, A. Inoue, T. Zhang, A. Sakai and T. Sakurai: Philos. Mag. Lett. **80** (2000) 263–269.
42) A. Inoue, T. Zhang, J. Saida, M. Matsushita, M. W. Chen and T. Sakurai: Mater. Trans., JIM **40** (1999) 1181–1184.
43) J. Saida, M. Matsushita and A. Inoue: Mater. Trans., JIM **41** (2000) 1505–1510.
44) J. Saida and A. Inoue: J. Phys. Condens. Matter. **13** (2001) L73–L78.
45) M. Imafuku, S. Sato, H. Koshiba, E. Matsubara and A. Inoue: Mater. Trans., JIM **41** (2000) 1526–1529.
46) M. Imafuku, K. Yaota, K. S. Sato, W. Zhang and A. Inoue: Mater. Trans., JIM **40** (1999) 1144–1148.
47) A. Inoue, T. Negishi, H. M. Kimura, T. Zhang and A. R. Yavari: Mater. Trans., JIM **39** (1997) 318–321.
48) A. Inoue, T. Negishi, H. M. Kimura, T. Zhang and A. R. Yavari: Mater. Sci. Forum **39** (1998) 318–321.
49) A. Inoue: Inoue Superliquid Project Guidebook, 1998.
50) N. Nishiyama and A. Inoue: Mater. Trans., JIM **38** (1997) 464–472.
51) N. Nishiyama, M. Horino, O. Haruyama and A. Inoue: Appl. Phys. Lett. **76** (2000) 3914–3916.
52) A. Takeuchi and A. Inoue: Mater. Sci. Eng. **A304–306** (2001) 446–451.
53) G. A. Mansoori, N. F. Carnahan, K. E. Starling and T. W. Leland, Jr.: J. Chem. Phys. **54** (1971) 1523–1525.
54) B. S. Murty, S. Ranganathan and M. M. Rao: Mater. Sci. Eng. **A149** (1992) 231–240.
55) Miedema: *Cohsion in Metals*, (eds. F. R. de Boer, R. Boom, W. C. M. Mattens, A. R. Miedema and A. K. Nissen, Elsevier Science Publishers B.V., Netherlands, 1988) pp. 1–758.
56) A. Takeuchi and A. Inoue: Mater. Trans., JIM **41** (2000) 1372–1378.
57) A. Takeuchi and A. Inoue: Mater. Trans. **42** (2001) 1435–1444.
58) K. Amiya and A. Inoue: Mater. Trans., JIM **41** (2000) 1460–1462.
59) A. Inoue and T. Zhang: Mater. Trans., JIM **37** (1996) 185–187.
60) A. Inoue, T. Zhang, A. Takeuchi: Appl. Phys. Lett. **71** (1997) 464–466.
61) A. Inoue, W. Zhang, T. Zhang and K. Kurosaka: Acta Mater. **49** (2001) 2645–2652.
62) *Supercooled Liquid, Bulk Glassy and Nanocrystalline States of Alloys* (eds. A. Inoue, A. R. Yavari, W. L. Johnson and R. H. Dauskardt, Materials Research Society: MRS Symposium Proceedings, Vol. 644, Materials Research Society 2001) pp. L.3.1-L4.9.6.
63) A. Inoue, T. Masumoto and N. Yano: J. Mater. Sci. **19** (1984) 3786–3795.
64) A. Inoue: *Bulk Amorphous Alloys*, (Trans Tech Publications, Zurich, 1999) pp. 1–146.
65) Y. Yokoyama, N. Nishiyama, K. Fukaura. H. Sunada and A. Inoue: Mater. Trans., JIM **40** (1999) 696–699.
66) K. Fujita, A. Inoue and T. Zhang: Mater. Trans. **42** (2001) 1502–1508.
67) K. Iwata, H. Minamiguchi, T. Yamaguchi, M. Ohnuki and A. Inoue: Matria Japan **38** (1999) 251–253 (in Japanese).
68) W. L. Johnson: *Bulk Metallic Glasses* (eds. W. L. Johnson, A. Inoue and C. T. Liu, Materials Research Society: MRS Symposium Proceedings, Vol. 554, Materials Research Society, 1999) pp. 311–339.
69) A. Inoue, T. Zhang and A. Takeuchi: Mater. Sci. Forum **262–2** (1998) 855–864.
70) A. Inoue, Y. Shinohara and J. S. Gook: Mater. Trans., JIM **36** (1995) 1427–1433.
71) A. Inoue, T. Zhang, T. Itoi and A. Takeuchi: Mater. Trans., JIM **38** (1997) 359–362.
72) W. Zhang and A. Inoue: Mater. Trans., JIM **41** (2000) 1679–1682.
73) S. Pang, T. Zhang, K. Asami and A. Inoue: Mater. Trans. **42** (2001) 376–379.
74) *Rapidly Solidified Alloys*, ed. by H. H. Liebermann, Marcel Dekker, New York, (1993) pp. 617–663.
75) A. Makino, A. Inoue and T. Mizushima: Mater. Trans., JIM **41** (2000) 1471–1477.
76) A. Inoue, H. Koshiba and T. Itoi: Mat. Sci. Forum **343–346** (2000) 81–90.
77) S. J. Pang, T. Zhang, K. Asami and A. Inoue: Acta Mater. **50** (2002) 489–497.
78) A. Inoue: *Bulk Amorphous Alloys*, (Trans Tech Publications, Zurich, 1998) pp. 1–116.
79) A. Inoue, Y. Kawamura and Y. Saotome: Mater. Sci. Forum **233–234** (1997) 147–154.
80) Y. Kawamura, T. Nakamura, H. Kato, H. Mano and A. Inoue: Mater. Sci. Eng. A **304** (2001) 674–678.
81) Y. Saotome and A. Inoue: *The 7th IEEE Int. Workshop on Micro Electro Mechanical Systems* (MEMS-94) (1994) pp. 343–348.
82) Olympus Co. Ltd, unpublished research, (1998).
83) A. Inoue and Y. Saotome: Metals **3** (1993) 51–57 (in Japanese).
84) Y. Saotome, K. Ito, T. Zhang and A. Inoue: Scr. Mater. **44** (2001) 1541–1545.
85) A. Inoue and S. Yuasa: unpublished research (2001).
86) C. Fan and A. Inoue: Mater. Trans., JIM **38** (1997) 1040–1046.
87) A. Inoue, T. Zhang, J. Saida, M. Matsushita, M. W. Chen and T. Sakurai: Mater. Trans., JIM **40** (1999) 1137–1143.
88) A. Inoue and X. M. Wang: unpublished research (1999).